

Parameters of Fast and High-Yield InAs/GaAs Quantum Dot Semiconductor Scintillator

A. Minns,¹ K. Dropiewski,¹ M. Yakimov,¹ V. Tokranov,¹ M. Hedges,³ P. Murat,² and S. Oktyabrsky^{1*}

¹ *SUNY Polytechnic Institute, Albany, NY*

² *Fermi National Accelerator Laboratory, Batavia, IL*

³ *Purdue University, West Lafayette, IN*

ABSTRACT

InAs quantum dots (QDs) embedded into a waveguiding GaAs semiconductor matrix may produce scintillation detectors with exceptional speed and yield, making them valuable for nuclear security, medical imaging, and high energy physics applications. In this work, we developed thick ($\sim 25\mu\text{m}$) epitaxial heterostructures with high luminescence efficiency composed of self-assembled nano-engineered InAs QDs grown by molecular beam epitaxy. The bulk GaAs acts as a stopping material for incident particles and as a waveguide when layer-transferred onto a low-index substrate. Waveguiding and self-absorption ($< 1\text{cm}^{-1}$) were studied using photoluminescence with scanning laser excitation and modeled with ray optics approximation and geometrical coupling of high-index waveguide to a collection fiber. Scintillating signals from α -particles were analyzed with an external photodiode (PD) and an integrated PD which provided an improved optical coupling. The mean charge collected by the integrated PD corresponded to 3×10^4 photoelectrons per 1 MeV of deposited energy, or $\sim 13\%$ of the theoretically achievable light yield. Combined with the previously measured QD scintillation time of 0.3-0.6 ns, this makes the InAs/GaAs QD heterostructures the fastest high yield scintillation material reported.

INTRODUCTION

Development of high light yield scintillating materials with picosecond time resolution is considered an enabling technology for multiple medical imaging, security sensing, and high-energy physics applications [1, 2]. Recently, a novel approach toward efficient and fast semiconductor-based scintillation materials was proposed [3, 4] and demonstrated [5, 6]. The approach utilizes quantum dots (QDs) as luminescent centers within a semiconductor host matrix and addresses several limitations of the existing inorganic scintillators. Semiconductors, such as CdTe or GaAs, due to their narrow bandgap compared to crystal scintillators [7] and low defect-related recombination, exhibit exceptionally high light yield ($\sim 2.4 \times 10^5$ photons/MeV for GaAs). The InAs/GaAs QD medium exhibits fast radiative recombination and high luminescence efficiency at room temperature, and if properly engineered, can provide fast capture of electrons and strong red-shift (> 300 nm) of photoluminescence from the GaAs absorption edge to reduce self-absorption [4]. The large refractive index of GaAs limits the escaped light to only about 2%, a natural solution to improving the light collection is to integrate a photodiode (PD) with the scintillating structure. Recent measurements of 5.5 MeV α -particles with such detector have demonstrated extremely fast, 0.3-0.6 ns, scintillations and the time resolution of 55-70 ps, limited by the system noise [5, 6].

In this work, we analyzed the light yield of 25 μm thick scintillation waveguides and quantified self-absorption and scattering losses of the QD luminescence. The light yield has been measured with the photodetector screened from direct photoionization, showing signal dependence on deposited energy.

MATERIALS AND METHODS

* Corresponding author's email: soktyabrsky@sunypoly.edu

The scintillation structures studied were grown with molecular beam epitaxy (MBE) on 3" GaAs (001) substrates and primarily consisted of 25 μm thick GaAs matrix layers with sparse sheets of InAs QDs. Some of the structures also contained an integrated InGaAs p-i-n photodiode (PD) on top of the scintillator.

The MBE growth process was started with a 100 nm thick AlAs sacrificial layer allow easy separation of the scintillation waveguide from the substrate (Fig. 1a). The bottom layer of the waveguide is 150 nm of variable bandgap p-type $\text{Al}_{0.3-0.1}\text{Ga}_{0.7-0.9}\text{As}$ semiconductor barrier to reduce surface recombination of the minority carriers. The scintillation waveguide is composed of repeating layers of 2 monolayer (ML) thick self-assembled InAs grown at 520 $^{\circ}\text{C}$, capped with a 2 ML of AlAs to control the shape of the QDs, improve uniformity and reduce wetting layer states [8]. Cross-sectional transmission electron microscopy (TEM) images of the QD layers in the structure are shown in Fig. 1(b, c). Owing to high lattice mismatch strain of 7%, InAs QDs self-assemble on the growing surface with density of about $3.5 \times 10^{10} \text{ cm}^{-2}$, have dome shape with lateral size of 14-18 nm (Fig 1b) and height of 5-6 nm. The InAs wetting layer (WL) typical for the Stranski–Krastanov mechanism of self-assembly was covered with a wider bandgap AlAs capping layer (Fig. 1c) which pushed the WL electronic levels above those of QDs thus reducing WL-related self-absorption. The QD medium was designed to provide fast capture of photoionized electrons into QDs (few ps), high QD luminescence efficiency at room temperature (>50%), and strong red-shift of photoluminescence (PL) from the GaAs absorption edge (>250 nm) [5].

The 800 nm thick GaAs intermediate layers grown at 590 $^{\circ}\text{C}$ were modulation p-type Carbon-doped to facilitate fast capture of electrons. Doping level was adjusted to achieve about 4 holes per QD as described in detail in Ref. [5]. To complete the scintillation waveguide, another 150 nm layer of variable AlGaAs is grown capped with 150 nm p-GaAs for protection against oxidation.

Tuned to the QD emission wavelength, the integrated PD is composed of $\text{In}_{0.35}\text{Ga}_{0.65}\text{As}$ layers grown at 450 $^{\circ}\text{C}$: a 300 nm n^{+} -type contact followed by a 700 nm undoped absorber layer and a 400 nm p^{+} -contact layer. The PD structure is grown on a 700 nm metamorphic graded comprised of $\text{Al}_{0.92-0.6}\text{In}_{0.03-0.35}\text{Ga}_{0.05}\text{As}$ grown at low temperature 350 $^{\circ}\text{C}$, intended to accommodate 2.5% misfit strain between GaAs and InGaAs. The bandgap of the PD absorber was adjusted to 0.95 eV at room temperature, which provides about 60% absorption of 1170 nm photons at a normal incidence. The PD is fabricated using two lithography masks to form the photodetector mesa and PD contact metallization.

The scintillators were characterized by transmission electron microscopy to visualize the microstructure of the material, by photoluminescence to assess optical properties of the QD waveguides and by α -particle induced

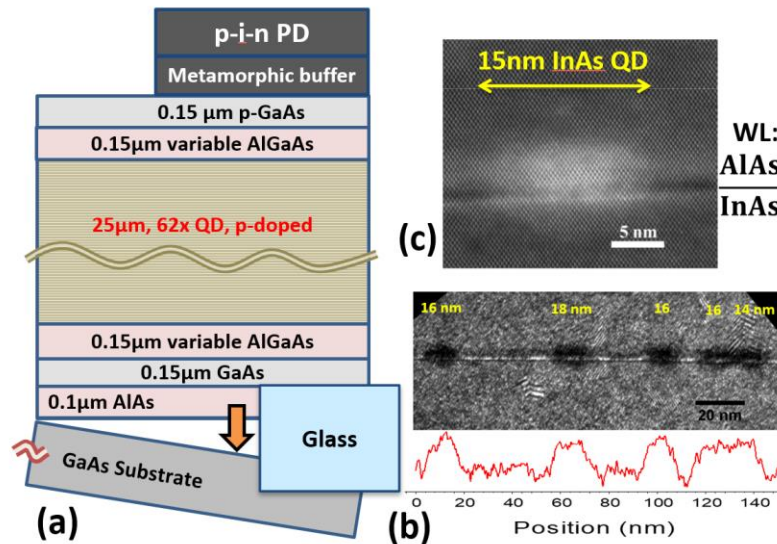


Figure 1. (a) Layout of an MBE grown structure of an InAs QD/GaAs waveguide (WG) with schematically shown InGaAs photodiode (PD) grown on top and GaAs substrate separation with epitaxial lift-off by dissolving the AlAs sacrificial layer. (b) Dark field cross-sectional image of a QD layer with contrast profile allowing for QD lateral size estimation. (c) Magnified high-angle annular dark field STEM image showing bright contrast of InAs QD and part of the wetting layer (WL) and dark contrast of the AlAs capping layer.

scintillation from an ^{241}Am radioactive source to evaluate light yield and collection efficiency of the structures. The chips of scintillation detectors with integrated PDs were wire-bonded to a printed circuit board (PCB) with transimpedance amplifier (TIA) based on OPA847 broadband operational amplifier and additional 50Ω gain block. Depending on the PD capacitance, the bandwidth of the TIA was 50-200 MHz. The PCB output was fed into a digital oscilloscope with 4 GHz bandwidth, and the data were further processed within a Matlab environment. The area under the signal waveform was taken to derive the observed collected charge. In all cases α -particle induced voltage pulse events were captured with trigger levels just above the background noise level.

In order to prevent direct photoionization of the PD depletion region, the chips released from the GaAs substrate were kept free-standing without glass carrier and were irradiated with α -particles from a side, opposite to the PD. Given the range of 5.5 MeV α -particles in GaAs is about 18 mm, the PD was entirely shielded from the radioactive source by the bulk of the QD scintillator.

The datasets generated and analyzed during the current study are available from the corresponding author on reasonable request.

RESULTS AND DISCUSSION

To evaluate light propagation in a QD waveguide (WG), a scintillation WG bar was excited with a red (650 nm) focused laser beam, and the photoluminescence (PL) spectra were measured by collecting the light with a $62.5\ \mu\text{m}$ fiber and further dispersing it with a grating monochromator. Fig. 2(a) shows the PL spectra collected during the longitudinal scan of the WG bar imaged in the inset of Fig. 2 with the laser beam. Along with the reduction of the overall PL intensity, a noticeable redshift of the spectra with the propagation length indicates relatively strong self-absorption of the higher-energy portion of QD emission band. Emission from the excited QW states below $\sim 1125\ \text{nm}$ is decaying most markedly, though its contribution to the overall intensity reduction is relatively low. Fig. 2(b) compares the normalized integrated intensity of collected light to the calculated profiles. The initial drop of the intensity is mostly due to a small diameter ($62.5\ \mu\text{m}$) of the fiber core and its low acceptance angle, 15.7° for numerical aperture $\text{NA}=0.27$. The acceptance cone angle inside the WG with high refractive index of 3.5 is just $\theta=4.4^\circ$; therefore, this geometry tests the light propagation very close to the WG axis. Higher-order propagation modes are not coupled to the fiber. The initial geometrical reduction of the collected light by the fiber with a diameter d occurs at the length less than $d/2\tan\theta = 7\ \text{mm}$ (note the scan begins at about 1 mm from the WG edge). At longer lengths the intensity is not changing as seen for a lossless WG (Fig. 2b). Adding WG losses, namely self-absorption and scattering due to reflection from the surfaces, using ray optics approximation [5] improves the fit and allows extraction of the WG parameters: $\alpha=0.82\ \text{cm}^{-1}$ and $\text{Sc}=3\text{-}5\%$ per reflection, respectively (Fig. 2b). It should be noted that the light collection efficiency is not very sensitive to the variations in surface scattering due to almost axial propagation of light collected

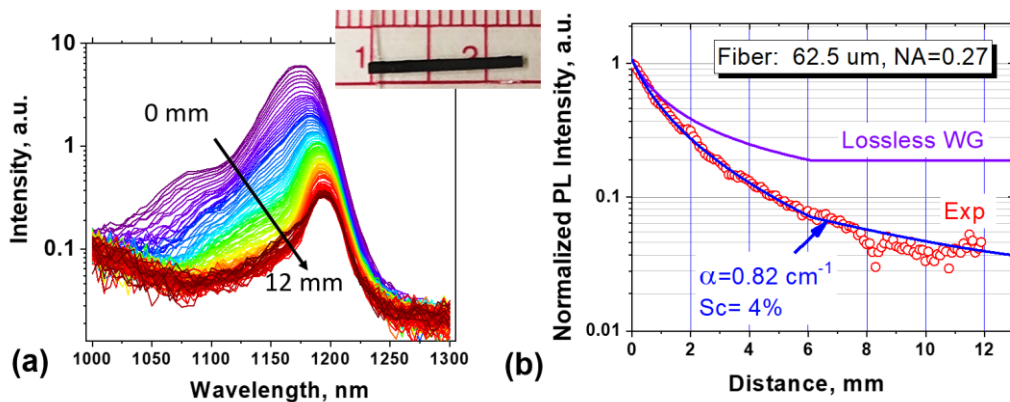


Figure 2. (a) PL spectra as a function of the light propagation distance in the WG as the excitation spot moves away from the collecting fiber. Inset shows a photograph of the WG with the size $13.8 \times 1.1 \times 0.025\ \text{mm}^3$ containing 31 QD sheets separated by 800 nm, transferred onto a glass slab. (b) Normalized integrated PL intensity picked up with an optical fiber comparing experimental data (symbols) to calculated signal (lines) from a lossless WG and the WG with the average absorption of $0.82\ \text{cm}^{-1}$ and scattering of 4% per reflection. Zero distance on the plot corresponds to about 1 mm from the edge of the WG.

by the fiber.

The scintillating response was analyzed using the experimental setup shown in Fig. 3(a), in which a QD scintillation layer was air-coupled to an external commercial $\text{Ø}300\ \mu\text{m}$ InGaAs PD. During fabrication, a $\sim 1 \times 1\ \text{mm}^2$ fragment of the structure was thinned, but not lifted off from approximately $150\ \mu\text{m}$ of the remaining GaAs substrate. The sample, GaAs substrate side down, was excited by $5.5\ \text{MeV}$ α -particles from a $1\ \mu\text{Ci}$ ^{241}Am radioactive source. A protective film and $5\ \text{mm}$ of air between the source and the device reduced the α -particle energy to $4\ \text{MeV}$. Firstly, the setup on the top (Fig. 3a) was used to collect scintillation responses. In this configuration, the PD was fully shielded from the direct ionization by both the scintillating layer and the substrate. Secondly, the scintillator was removed to measure the effect of direct photoionization in the PD. Finally, the noise was measured with the radioactive source removed. The difference in the pulse amplitudes and widths is clearly seen in the oscillograms in Fig. 3(b). The pulse width of $\sim 3\ \text{ns}$ is determined by $\sim 10\ \text{pF}$ capacitance of the PD and is significantly longer than the QD lifetime of $\sim 0.5\ \text{ns}$ [5, 6].

Fig. 3(c) shows a good separation between the three types of events in the collected charge vs. peak voltage plane. Direct PD ionization events (red) gave the highest peak voltage and up to 10^5 electrons of collected charge due to narrow bandgap of $\text{In}_{0.53}\text{Ga}_{0.47}\text{As}$ PD that should generate 1.2×10^5 pairs/ μm by $4\ \text{MeV}$ α -particle. The high refractive index of GaAs limits light propagation through a planar interface with air, due to total internal reflection, to approximately 2 % of spatially uniform QD scintillation. This matches the observed maximum collected charge (black dots) of 10^4 electrons, corresponding to a collection efficiency of $\sim 1\%$.

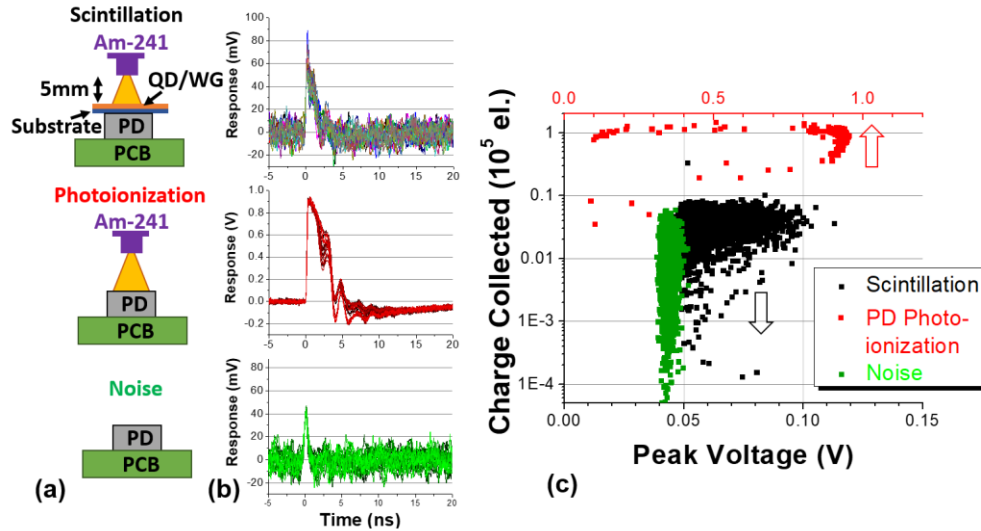


Figure 3. (a) Experimental setups used to collect scintillation results with external PD air-coupled to THE scintillator. (b) Traces of photocurrent response amplified with $10\ \text{k}\Omega$ transimpedance + $10\times$ voltage amplifiers for each experimental setup. (c) Distributions of charge plotted versus the peak voltage for the three experimental configurations shown in Fig.(a). Direct PD photoionization peak voltage axis is in red, on top.

To improve the light collection efficiency, an integrated PD was processed on the top surface of the waveguide. To avoid direct photoionization of the PD, the wire-bonded devices were irradiated with α -particles from the backside, as shown in Fig. 4(a). Distributions of charge collected by the PD appear bi-modal and change significantly with the distance between the ^{241}Am source and the detector (Fig.4b). As the source is moved away from the detector, the high-charge peak moves towards lower values showing its sensitivity to the α -particle energy that reduces with air ionization. The relative fraction of events in the peak increases as the readout threshold cuts off more and more events with α -particles hitting the detector not directly above the photodiode.

In contrast, the low-charge part of the distribution stays relatively intact. It is populated by events where the α -particles strike elsewhere other than over the PD (Fig.4a). In those events, the photons collection efficiency by the PD is lower, and the corresponding signals are more likely not to surpass the readout threshold.

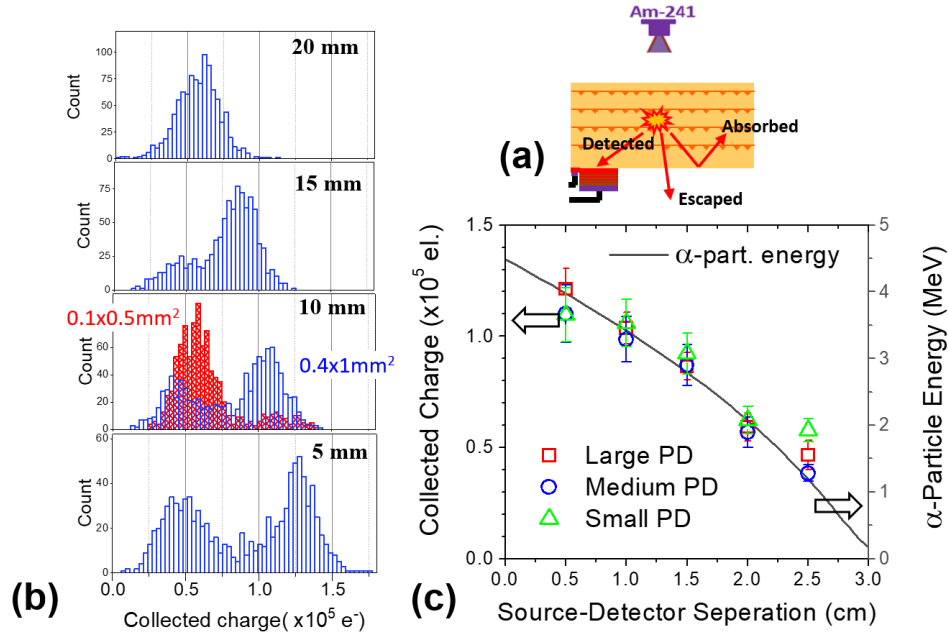


Figure 4. (a) . Schematics of backside α -particle irradiation; the patterned photodiode layers are protected from particles by the $>20 \mu\text{m}$ scintillator medium. Note the projection range of 5.5 MeV α -particles in GaAs is about 18 μm . (b) Experimental histograms of α -particle charge collection into a large $0.4 \times 1 \text{ mm}^2$ PD integrated with QD scintillator placed at different distances from the α -particle source. Histogram from a medium $0.1 \times 0.5 \text{ mm}^2$ PD at 10 mm separation is overlapped for comparison. (c) Average collected charge by different devices from ^{241}Am radioactive source. The original energy of the α -particles is slightly decreased in the source protection layer. Solid line is an energy attenuation curve of 4.8 MeV α -particles in air. The charge averaging was performed for high-energy peaks in the histograms which correspond to minimal photon travelling paths when an α -particle impinges the waveguide directly over the PD.

Fig. 4(c) shows the average charge collected by PDs with different areas as a function of the source-detector distance. As α -particles travel in the air, their energy is reduced due to ionization as shown by the solid curve. The energy of the α -particles emitted by the source was calibrated in vacuum against backscattered He^+ from gold film using Ge detector. The average energy was 4.8 MeV, lower than the decay energy due to losses in the source protection layer. The charge averaging was performed exclusively for high-charge peaks by subtracting the low-charge peak from the histograms. A good matching of the PD charge to the α -particle energy loss curve confirms the validity of the presented analysis. The measurements yield 3×10^4 photoelectrons per 1 MeV of deposited energy, which corresponds to $\sim 13\%$ of the theoretically achievable limit in the InAs/GaAs QD system. Together with the QD luminescence emission time $\tau \sim 0.3\text{-}0.6 \text{ ns}$ measured in [5], this makes the QD-based scintillators the fastest high yield scintillating materials reported so far.

CONCLUSIONS

Optical and scintillating properties of the InAs/GaAs QD waveguiding nanomaterial were studied using photoluminescence with scanning laser excitation and modeled under ray optics approximation and geometrical coupling of a high refractive index waveguide to a collection fiber. Self-absorption of the QD emission is estimated at as low as 0.8 cm^{-1} which is a result of AlAs capping of QDs. Scintillation signals from 5.5 MeV α -particles were measured with both external and integrated PDs, the latter provided an improved optical coupling. The charge collected by the integrated PD, 3×10^4 photoelectrons per 1 MeV of deposited energy, corresponds to about 13% of theoretically achievable limit in this material. This value, combined with previously measured emission time of 0.3-0.6 ns, makes the InAs/GaAs QD heterostructure the fastest high yield scintillation material reported so far.

ACKNOWLEDGEMENTS

This work was supported by National Science Foundation under award DMR-1511708637 and the U.S. Department of Energy, Office of Science under award DE-SC0019031.

REFERENCES

- [1] P. Lecoq, Nuclear Instruments and Methods in Physics Research A, 809 (2016) 130-139.
- [2] Z. Wang, E. Guardincerri, D. Rathman, M. Azzouz, C.W. Barnes, R. Berger, E. Bond, D. Craig, D. Holtkamp, J. Kapustinsky, Hard X-Ray, Gamma-Ray, and Neutron Detector Physics XV, Int. Soc. Optics and Photonics, 2013, pp. 88521A.
- [3] S. Luryi, Int. J. High Speed Electronics and Systems, 18 (2008) 973-982.
- [4] S. Oktyabrsky, M. Yakimov, V. Tokranov, P. Murat, IEEE Trans. Nuclear Science, 63 (2016) 656-663.
- [5] K. Dropiewski, A. Minns, M. Yakimov, V. Tokranov, P. Murat, S. Oktyabrsky, J. Luminescence, 220 (2020) 116952.
- [6] K. Dropiewski, A. Minns, M. Yakimov, V. Tokranov, P. Murat, S. Oktyabrsky, Nuclear Instruments and Methods in Physics Research A, 954 (2020) 161472.
- [7] S.E. Derenzo, E. Bourret-Courshesne, G. Bizarri, A. Canning, Nuclear Instruments and Methods in Physics Research A, 805 (2016) 36-40.
- [8] A. Varghese, M. Yakimov, V. Tokranov, V. Mitin, K. Sablon, A. Sergeev, S. Oktyabrsky, Nanoscale, 8 (2016) 7248-7256.